Validation of Multiple Hypothesis RAIM Algorithm Using Dual-frequency GNSS Signals

Alexandru Ene, Juan Blanch, Todd Walter, J. David Powell
Stanford University, Stanford CA, USA

BIOGRAPHY

Alexandru Ene is a Ph.D. candidate in Aerospace Engineering working in the Global Positioning System (GPS) Laboratory at Stanford University. His research focus is software simulation in the area of combined GPS/Galileo signals, positioning error threat space and integrity. He holds a Bachelors degree in Astronomy and Astrophysics and a citation in German Language from Harvard (2002), and a Masters degree in Management Science and Engineering from Stanford (2006).

ABSTRACT

A Multiple Hypothesis Solution Separation (MHSS) RAIM algorithm was developed at Stanford in recent years, with the purpose of meeting the stringent integrity requirements imposed by the Federal Aviation Administration (FAA) and International Civil Aviation Organization (ICAO). When satellite navigation is the primary means for guidance of civil aircraft, it has to meet the strict requirements for the landing and take-off phases of flight. In previous work, it was demonstrated in simulation that the Stanford MHSS algorithm is capable of achieving a better performance than is required of LPV 200 approaches worldwide, with sufficient availability. [Blanch et al. 2007, Ene et al. 2007]

The goal of this work is to continue testing and calibrating an optimized MHSS algorithm with dual-frequency flight data obtained by courtesy of the FAA Technical Center. An important part of this process is verifying that the theoretical model previously used in simulation for the magnitude of satellite range errors and biases is realistic and when compared with actual measurements. The flight data will be the most instrumental in comparing the simulated model with actual in-flight conditions.

Once the phase of developing a realistic model of the actual errors is complete, the MHSS algorithm will be validated with independent flight test data under nominal conditions. The final goal of these validation procedures is to compare the performance of unaided MHSS RAIM with RTCA-229D requirements, and also to assess the realistic performance capabilities of future Global Navigation Satellite Systems (GNSS) under multiple possible scenarios in terms of the overall number of operational satellites and constellations.

INTRODUCTION

Vertical errors are critical during aviation precision approaches, and they are also generally greater than horizontal errors for satellite-based positioning, because of the inherent geometry between the receiver and the ranging sources. The purpose of this work is to evaluate the performance of an unaided dual-frequency satellite constellation from a vertical integrity standpoint for aviation precision approach. Its intent is to complete a previous study [Ene 2007] investigating what Vertical Protection Level (VPL) values could be achieved with Receiver Autonomous Integrity Monitoring (RAIM) under realistic flight test conditions. The focus of the current study will be on understanding what are the differences, if any, between the assumptions previously made while testing the performance of the MHSS RAIM algorithm in simulation under different scenarios, and the factors that influence the performance of unaided RAIM when actual GPS measurement data is being used.

The set of measurements used in this paper was taken on September 19, 2006 during a test flight from the Memphis, TN airport in the USA, between approximately 17:30 and 20:00 UT. The aircraft used was a Boeing 727, property of the United States FAA. Data was made available to Stanford University by the FAA Tech Center (http://www.nstb.tc.faa.gov/) for both an Ashtech Z-Extreme and a NovAtel OEM4 receiver onboard the aircraft, as well as another NovAtel OEM4 receiver located on top of a hangar on the ground, used as reference. RINEX raw measurement files were provided as well as the processing results for the single-frequency "truth" differential GPS position solution, using available Wide Area Augmentation System (WAAS) corrections. This position estimate was used as reliable estimate of the airplane trajectory during the test, and also as a reference against which independent in-house processing results of the same data were compared.

This work will summarize the steps taken in the unaided processing of the in-flight GPS measurements and obtaining of a dual-frequency position solution. Subsequently, a VPL value will be determined at each point in time during the recorded flight, in the same way integrity monitoring results would be obtained in real time. By comparing the dual-frequency position solution to the "truth" reference, a relatively precise estimate of the Vertical Positioning Error (VPE) can be determined

in order to assess how the error values compare with the protection level, guaranteed to bound the error with a probability of $1\text{-}10^{-7}$. The main body of the ensuing discussion will be dedicated on understanding how the assumptions made about the size of the satellite ranging errors under nominal conditions compare to the observed errors. The accuracy of error modeling can be a determining factor on whether the RAIM algorithm produces protection levels that are realistic or over-conservative. Future studies will use additional flight data sets to validate the use of an appropriate error model.

DATA PROCESSING ALGORITHM

Initially available GPS observation data includes the raw code and carrier pseudoranges at each of the two existing broadcast frequencies, the L1 and L2 bands. While the carrier measurements are affected by an integer ambiguity in terms of the exact number of carrier wavelengths included in the pseudorange, they are also affected by a relatively lower overall level of root-mean-square (RMS) noise. It is therefore to one's advantage to pass the code pseudorange measurements through a smoothing filter based on the available carrier observations, before using the ranging data to determine a position solution for the user. Both the L1 and L2 code pseudoranges will be smoothed by the corresponding carrier measurements before being combined in turn to yield an ionosphere-free range measurement:

$$\rho_{IF} = (\gamma \cdot \rho_{L1} - \rho_{L2}) / (\gamma - 1) \quad (1)$$

where γ is a coefficient dependent on the center frequencies of the L1 and L2 signals: $\gamma = (f_{L1}/f_{L2})^2$, and ρ_{L1} and ρ_{L2} represent the values of the smoothed pseudoranges corresponding to the two frequency bands.

The greatest challenge during this process is that four different values of the distance between each satellite and the receiving user antenna (i.e. user range measurements) are available at every point in time, and these four measurements do not always agree closely. One main source of disagreement between corresponding measurements at the L1 and L2 frequencies is the amount of ionospheric delay that affects the propagation of each signal. However, the observations are also affected by errors stemming from the receiver's ability to track the satellite signal at each of the two frequencies, and these errors can at times prove significantly larger than the difference in the propagation delays. The carrier measurements can be affected by the uncertainty in estimating the exact number of integer cycles included in the pseudorange measurement at each frequency, and sudden changes in the integer estimate can affect the two frequencies the same way or in different amounts. It is therefore important that a cycle slip detector is implemented for each of the carrier measurements before they are used in turn for smoothing the code observations. Since none of the four types of measurements can be used as a reference for the other three, given how they could be each affected by errors with significantly different magnitudes, the most effective way to build cycle slip detection into the process is by comparing each measurement with previously available historical values

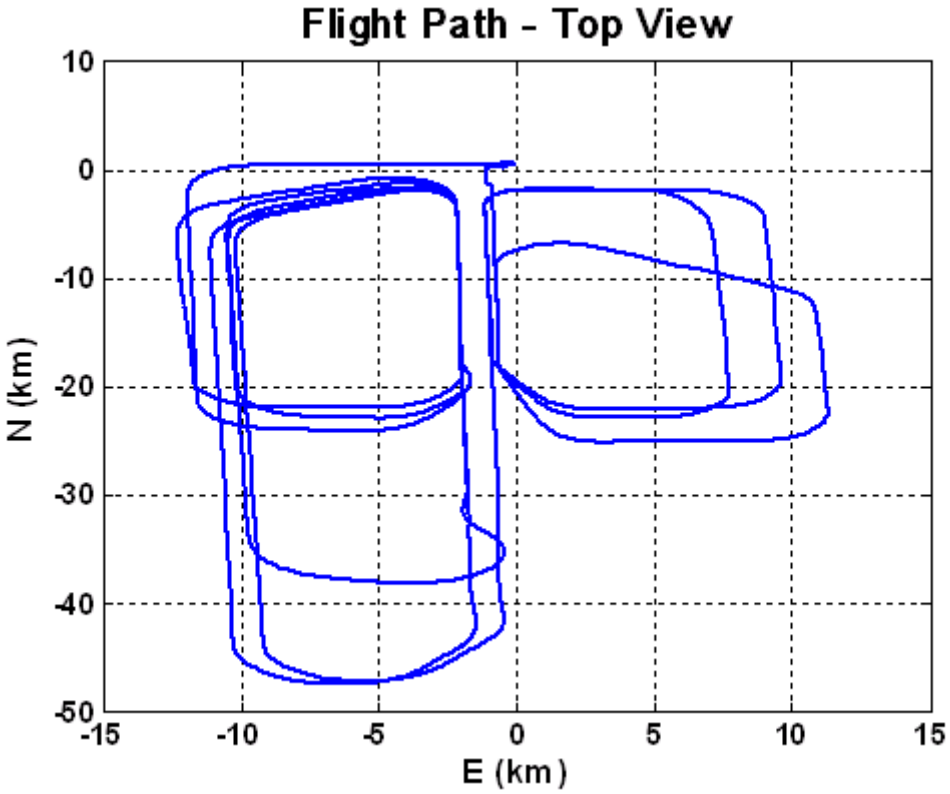

Figure 1. Trajectory of the inspection flight at Memphis airport on the 19th of September, 2006. Distances are in kilometers with the North direction being up. The maximum flight altitude was less than 1000m, as the aircraft did a succession of takeoffs and landings.

of itself. It is expected that range measurements exhibit a smooth continuous variation in time, due to the relative motion between the ranging source (i.e. GPS satellite) and the user receiver. Therefore, it will be assumed that the speed at which these range measurements vary should be practically constant over a short period of time and roughly equivalent to the dominating term in the relative velocity, which is the speed of the satellite motion relative to a reference point on the Earth surface. Generally, this speed is considerably greater than any reasonable velocity of the user itself with respect to the ground, and it can be determined approximately based on knowledge of the satellite in-orbit dynamics. For reference, a trajectory of the aircraft motion relative to the ground is provided in Figure 1. For the purpose of cycle slip detection in the carrier range measurements, it was determined empirically that setting a threshold of 12.5 m/s^2 could effectively help distinguish between natural satellite-user relative motion and errors introduced by sudden jumps in the value of the integer ambiguity estimate at the receiver. Since there is a difference of several orders of magnitude between pseudorange variations caused by cycle slips as opposed to the natural motion of the positioning signal emitter and receiver, the use of an approximate threshold proves an effective method of detecting so-called cycle slips (Figure 2).

In addition to very sizable jumps in the raw pseudorange measurement for each satellite, cycle slips can also cause a temporary loss of lock in the receiver tracking loop, therefore also introducing smaller scale errors in the equivalent pseudocode-based range measurements. This introduces the additional need of monitoring for unusual variability in the code measurements as well. Any such conspicuously erroneous variability will cause the removal from consideration of ranging measurements at those points in time, in order not to introduce unjustifiably large errors in the ensuing user position solution. Based on the high correlation between these large errors in the code measurements and the cycle slips detected in the equivalent carrier measurements, the decision was made to eliminate observations related to a particular satellite for a short amount of time following the detection of a cycle slip in the carrier measurements. This period of time will be proportional to the averaging constant of the smoothing filter that is used.

The process of going between the raw GPS measurements and determining the user position solution starts with importing the information from the RINEX ephemeris and observation files into MatLab. Subsequently, the carrier range measurements are differentiated between each successive pair of 5Hz measurements for the same satellite, in order to obtain the velocity and acceleration of the carrier pseudorange variation. Cycle slip detection is first employed (Figure 3) and afterwards 100-second carrier smoothing of the code pseudoranges is performed, such that the higher-amplitude noise level in the pseudocode measurements is attenuated. Unusually large ranging errors are generally observed in both L1 and L2 as the receiver is trying to recover after each cycle slip and reacquire phase lock. In this meantime, the smoothing filter is also in the process of settling to an equilibrium state. In order to avoid introducing additional ranging errors through the carrier smoothing process, the 100s filter is reset immediately after a detected slip and the following 30s of measurements are discarded. The L1-L2 iono-free pseudorange is then formed from the combination of the two single-frequency smoothed pseudoranges, according to equation (1). The processed measurement data is further decimated to match the sampling time of the given reference truth position, available at a 1Hz rate.

The next step is to compute pseudorange corrections for the measurements according to the GPS Interface Specification document [IS-GPS-200D]. Ionospheric delays have already been removed through dual-frequency processing and the differential group delay (T_{GD}) correction does not need to be applied for the case of multiple frequencies. Based on the available ephemeris information, values can be computed for the satellite clock bias, as well as the tropospheric corrections, according to IS-200D 20.3.3.3.3.1 and the WAAS MOPS Appendix A.4.2.4 [RTCA DO-229D] respectively (Figure 4). Additionally, values of the "true" range between the user and each satellite, and a weighted average estimate of the user clock bias at each time epoch will be computed based on the available "truth" user location. These latter two values will be used in order to make an accurate determination of the User Range Error (URE) due to residual error sources such as satellite clock and ephemeris, atmospheric propagation and multipath. As an aside, it is important to mention that any current problems with semicodeless L2 signal acquisition generating large range errors are expected to significantly improve when independent pseudocode acquisition and tracking will be available at each different civilian broadcast frequency (e.g. L1, L2 and L5 for future modernized GPS signals).

Finally, a Weighted Least Squares (WLS) dual-frequency position solution will be computed for the flight inspection airplane, making it possible to estimate both the positioning errors and the ranging errors to each satellite in view at every instant during the data collection timeframe. The final value for the ranging error to each satellite will be obtained according to:

$$\boldsymbol{\varepsilon = \rho - r - I - T + B - b} \quad \textbf{(2)}$$

Here, ρ represents the initial single-frequency carrier-smoothed pseudorange, r is the geometric distance between the "true" user position and the satellite position according to the ephemeris information, I and T represent the iono and tropospheric delay corrections, while B and b are the estimated satellite and user clock biases respectively. The WLS weighting matrix will be the inverse of the covariance matrix for the ranging errors, assuming these errors can be approximated as normally distributed and uncorrelated. Consequently, the covariance matrix will be diagonal, with the elements corresponding to the expected variance for the error along each line of sight between the user and a given satellite. The initial model for this variance was agreed upon in

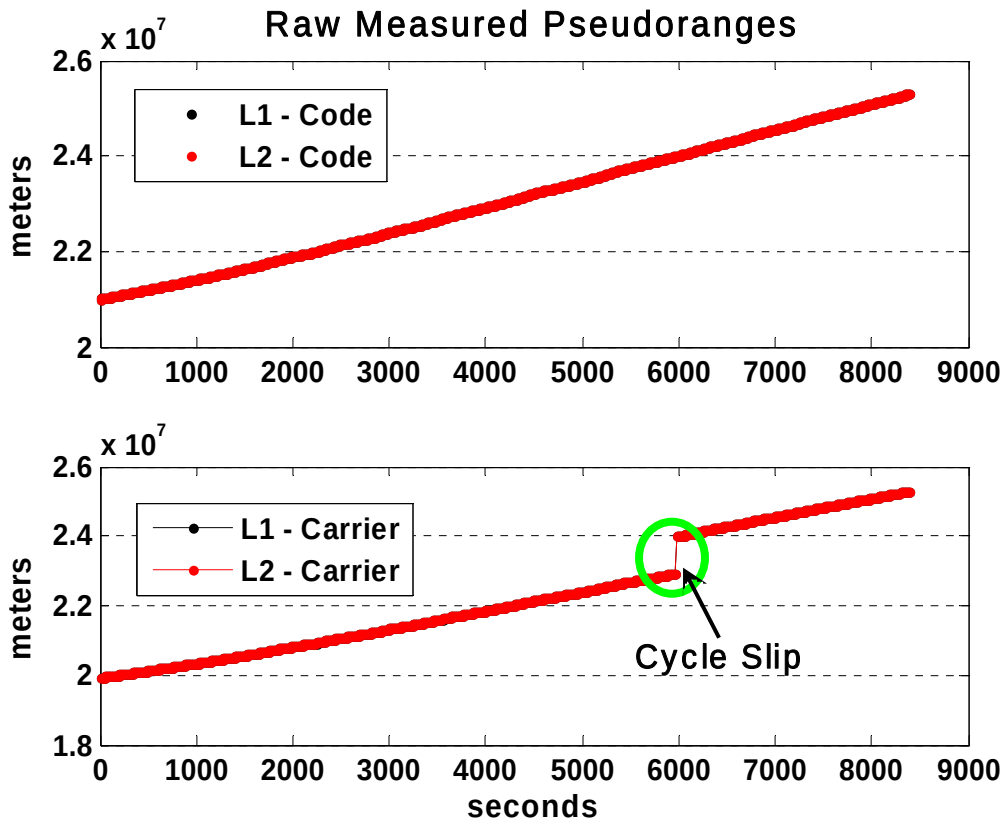

Figure 2. PRN16 code and carrier pseudoranges as observed by the Novatel receiver on the aircraft. The differences between the L1 and L2 pseudorange measurements are insignificant compared to the total range variation over the observation period – approximately 4000km in total. A carrier cycle slip is exemplified in the bottom plot, involving a ranging error of about 1000km.

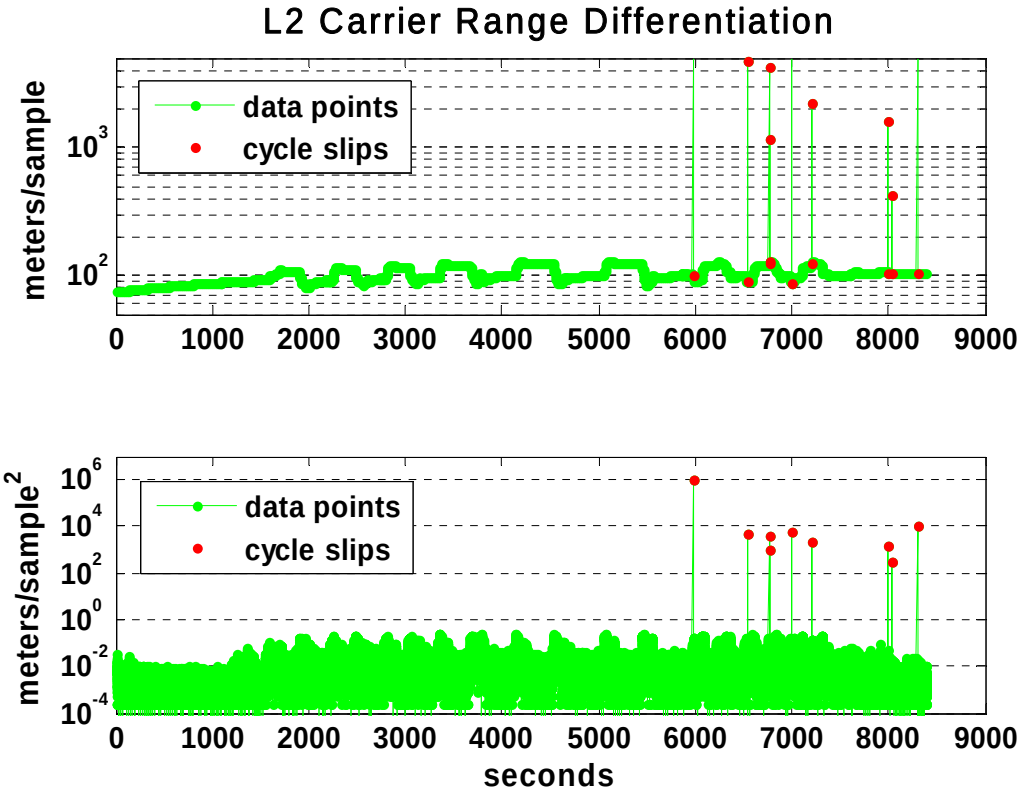

Figure 3. Sample output of the cycle slip detection algorithm for PRN16 observed with the Novatel receiver. The top plot illustrates the variation in the carrier range between each pair of successive measurements (notice how the 1000 km jump in the measured pseudorange value is off the scale). The bottom logarithmic plot illustrates the difference between successive samples on the top plot.

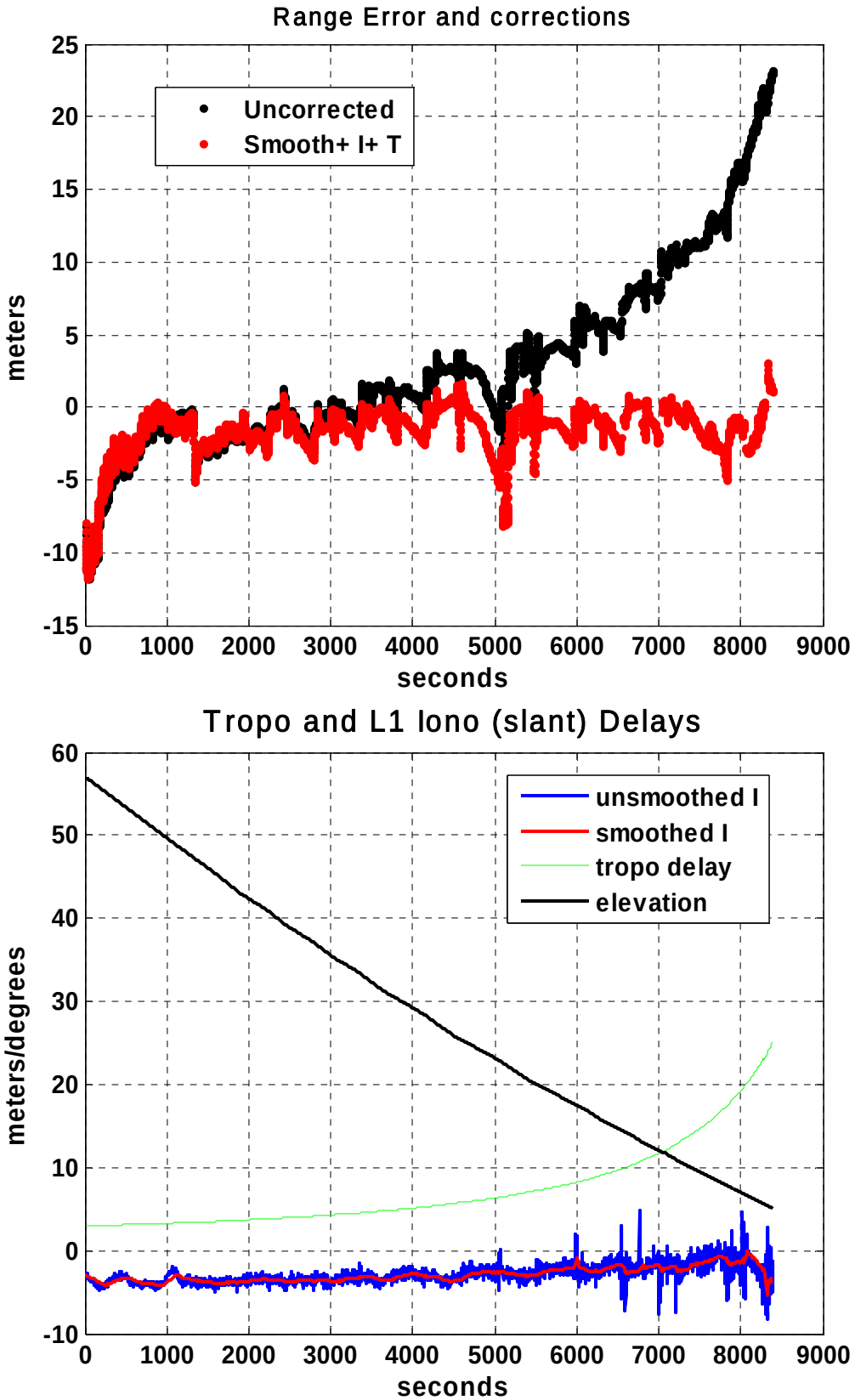

Figure 4. While accounting for the satellite clock bias on PRN16, the difference between the L1 code pseudorange measured by the Novatel receiver and the "true" range is given in the top plot. The effect of carrier smoothing and applying corrections for the ionospheric and tropospheric propagation delays is illustrated by displaying the black and the red curves side-by-side.
The bottom plot shows the satellite elevation (in degrees), the amplitude of the applied tropo correction, as well as the L1 ionospheric delay (computed as the difference between the L1 carrier range minus the iono-free pseudorange) before and after the smoothing process. Note that the L1-L2 Inter-frequency Bias (IFB) was not explicitly accounted for, causing the iono delay values to appear slightly negative. These readings can be easily separated in a positive delay plus a bias.

PRN	# Slips	Max Track (s)	Tot Track (s)	Avg Track (s)
1	18	1594.6	2876.8	137.5
3	0	8397.2	8397.2	8397.2
7	34	5974.0	7574.4	221.4
8	28	533.4	5720.0	99.1
10	79	272.4	1715.2	21.1
11	68	519.6	2943.2	27.2
13	0	8397.2	8397.2	8397.2
16	18	5971.4	8333.4	457.7
19	0	8397.2	8397.2	8397.2
20	30	3085.0	5003.2	166.8
23	0	8397.2	8397.2	8397.2
25	29	2776.8	5113.6	170.6
27	0	8397.2	8397.2	8397.2
28	20	499.8	3938.6	76.6

Table 1. Summary of cycle slips detected for the Novatel receiver, in both the L1 and L2 bands simultaneously. The values for the longest period of continuous tracking (Max Track), the total period that the satellite is in view (Tot Track) and the average length of tracking (Avg Track) are also provided. PRN10, which is the most affected by cycle slips, is also the only satellite that never rises above the mask angle during the observation period.

FAA GPS Evolutionary Architecture Study (GEAS) Panel meetings, and assumes a User Range Accuracy (URA) standard deviation of 1m and no ranging biases:

$$\sigma^2 = \sigma_{URA}^2 + \sigma_{tropo}^2 + \sigma_{iono\text{-}free}^2 \quad (3)$$

In the above equation, σ_{URA}^2 represents the variance of the range component of the signal-in-space (SIS) clock and ephemeris error, σ_{tropo}^2 is the assumed variance of the tropospheric range error after the corresponding tropospheric correction has been applied, and $\sigma_{iono\text{-}free}^2$ is the assumed variance of the ionosphere-free combination of the L1 and L2 measurements, representing a weighted combination of the σ_{air}^2 terms at the two frequencies. In turn, σ_{air}^2 is the sum of the assumed variances for the multipath error and the RMS background Gaussian noise in the receiver. The above error model was adapted from an initial model proposed by The MITRE Corporation [Lee et al. 2005].

RESULTS AND DISCUSSION

Due to the fact that more than half of the 14 satellites in the data set were either rising or setting and only 6 of the satellites reach elevations of 45° or higher during the approximately 140-minute flight inspection, the available measurements contain a relatively high number of cycle slips (Table 1). The cycle slips are a consequence of receiver loss of carrier lock, an event especially common at elevations below 15°, when the atmospheric attenuation of the GPS signal is the strongest. With a single active constellation for measurements, it is difficult to have more high-elevation satellites in sight providing high-quality ranging to the user. Despite this shortcoming, it was possible to remove most of the ranging error relying solely on the GPS Interface Specification document and on available models for error estimation and correction. Even in the absence of precise SBAS corrections, it was possible to obtain 3D position solutions mostly within 10m of the "truth" reference user location. The accuracy is visibly sensitive to the number of satellites used for positioning estimation, such that errors tend to get above 10m only when the number of ranging sources drops to 8 or less (Figure 5).

In order to compare the ranging errors observed during the flight test data collection with the magnitude of the errors expected according to the model used in previous simulation studies, a post-processing statistic of the measured errors was assembled. At first, the ranging error time history was analyzed for each different satellite (Figure 6) and a first-order fit of the data was performed. Based on this linear fit over the entire observation period for each PRN, the clock and ephemeris errors for the respective satellite were estimated and then removed from the overall range error, ε. The results were then combined across all satellites and allocated into bins of the satellite elevation ranging between 5° (which is the mask angle employed in this analysis) and 90° (zenith). The standard deviation of the remainder of the error and its mean, representing a small residual bias, were subsequently computed and compared to the root-square-sum (RSS) of the 2nd and 3rd terms in equation (3), which are also dependent on elevation. A summary of this comparison is offered in Table 3.

In the end, the WLS error residuals were used to also compute predicted error bounds for the airplane user, according to the MHSS RAIM algorithm developed at Stanford University [Blanch et al. 2007, Ene et al. 2007].

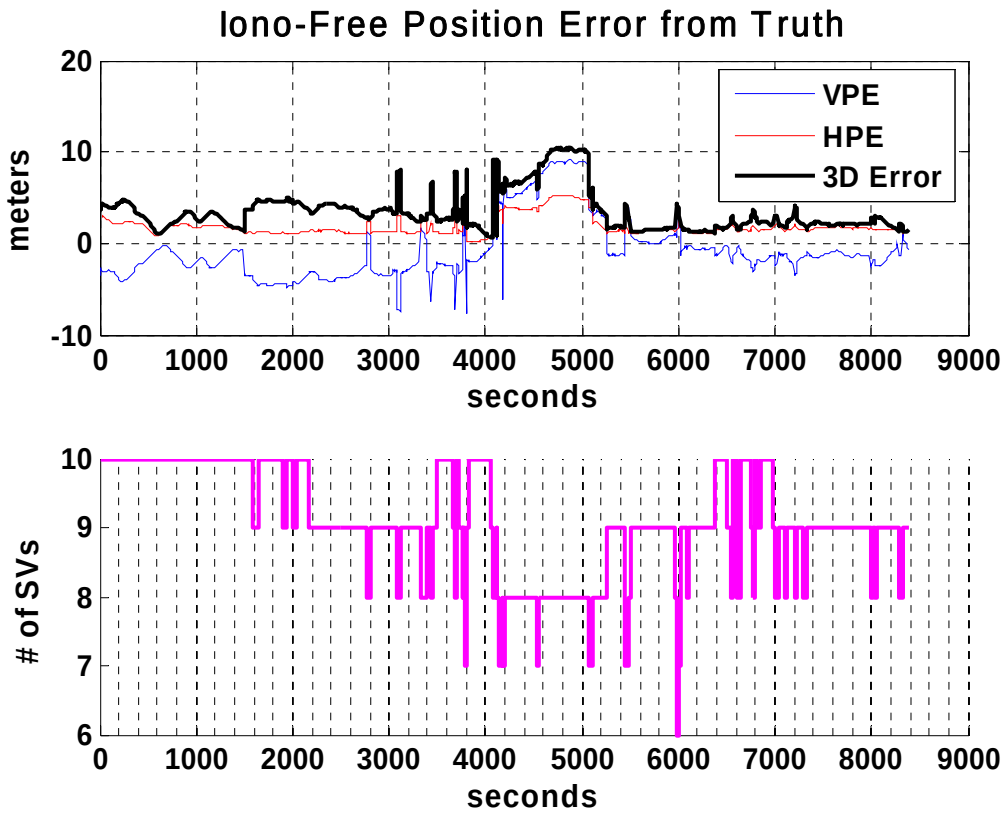

Figure 5. The Position Error values in the vertical (VPE) and horizontal (HPE) directions, as well as the overall position errors (top) are displayed in correlation to the plot of the total number of satellites included in the position solution (bottom).

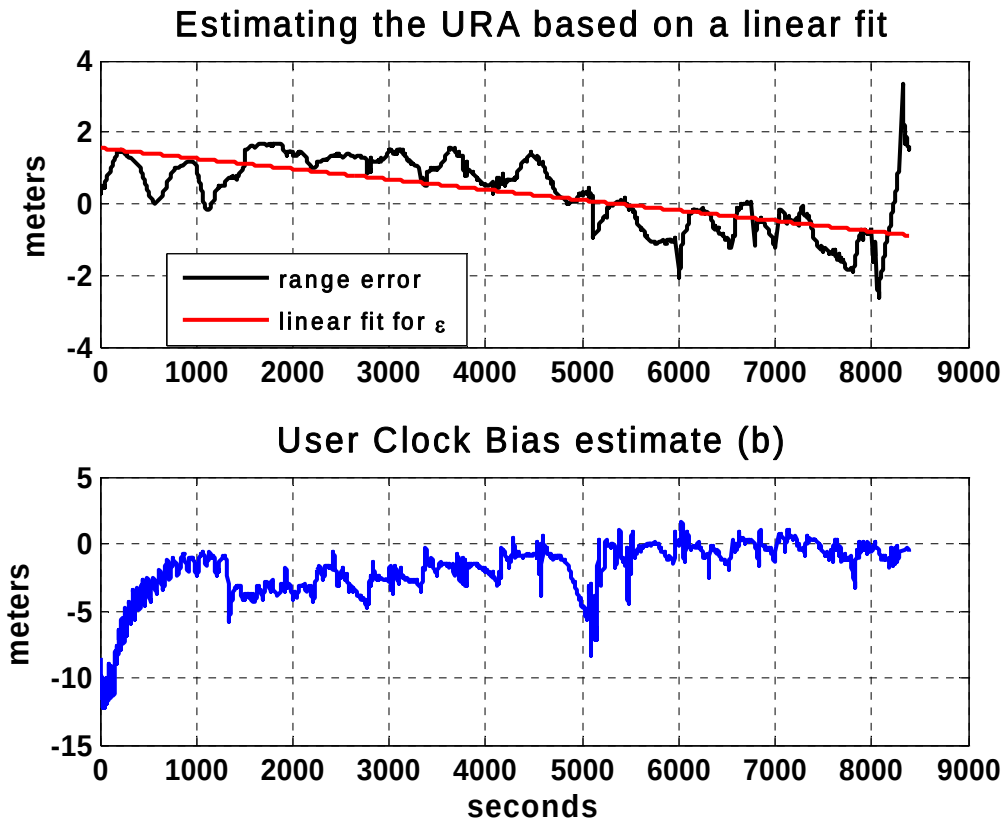

Figure 6. (Top): Linear fit for approximating the SIS ranging error for PRN 16.
(Bottom): The estimated value for the clock bias of the Novatel OEM4 flying onboard the aircraft, which has been subtracted from the range error after the application of the corrections in Fig. 4.

CONCLUSIONS

In terms of the performance of the RAIM algorithm, it can be seen from the comparison of the VPE to the VPL value (Figure 7) that the predicted protection level provides a safe margin in terms of bounding the vertical error for the duration of the flight test. However, the maximum value of the VPE/VPL ratio can be seen as quite large given the period of observations is only about 140 minutes and the required probability of providing Hazardously Misleading Information should be less than 1 in 10 million. The error model assumed in the VPL computation is however significantly different from the

Position Error from "Truth"		
	Mean	STD
Vertical	-0.776	3.427
Horizontal	1.858	1.064
3D	3.452	2.238

Table 2. Statistics of the positioning errors illustrated in Fig. 5 above.

# samples	Elevation less than:	Sigma	Bias	No URA Modeled sigma
	5			1.697
15201	15	0.983	-0.003	0.795
13836	25	1.193	0.099	0.539
10580	35	1.264	-0.361	0.440
8373	45	1.086	0.101	0.399
11730	55	0.667	0.025	0.379
10322	65	0.380	0.068	0.370
4501	75	0.310	0.173	0.365
2740	90	0.526	-0.042	0.361

Table 3. Ranging errors were reduced by a linear fit as shown in Fig. 6, binned by elevation and normal distribution statistics were computed for each bin and compared to the given error model.

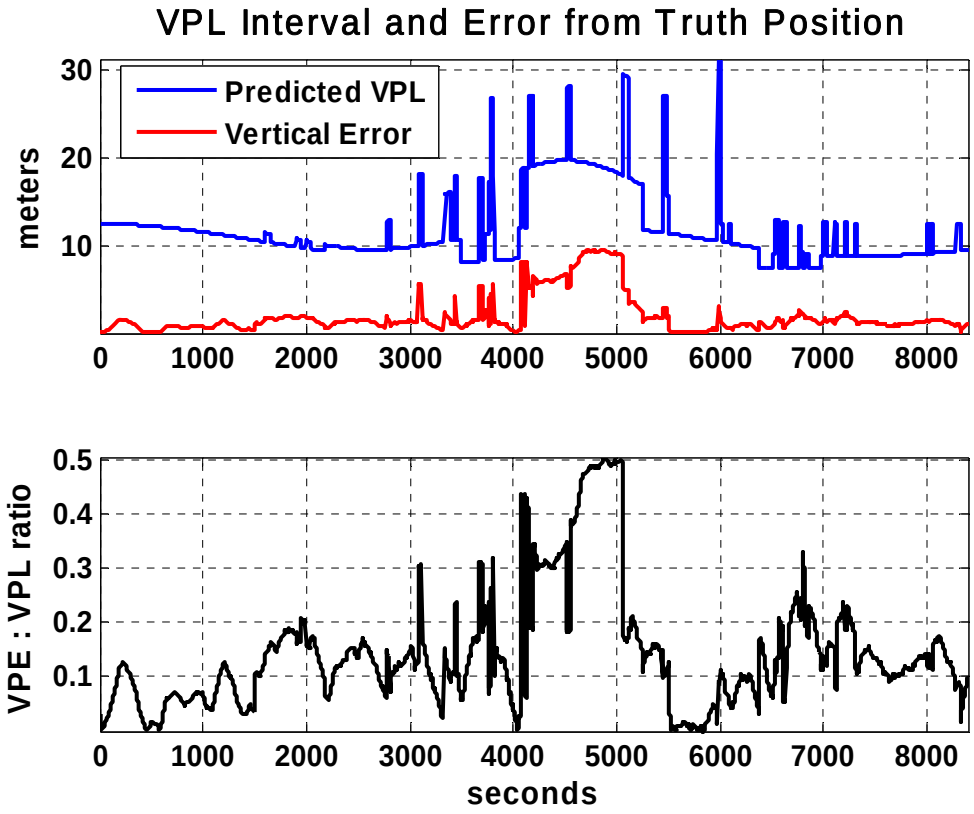

Figure 7. Results illustrating the comparison between the absolute errors (VPE) and the error bounds predicted by the MHSS RAIM algorithm (VPL) in vertical direction.

errors observed from the measurements with the two receivers (Figure 8). Additional analysis will be needed in order to align the existing error model to the type of errors observed during the L1-L2 dual frequency measurements. It is expected that the use of more realistic parameters as part of the theoretical error model will allow maintaining the highest possible standards of safety for the user. A future investigation is therefore planned with the purpose of further verification of the overall error model and finding the most appropriate values for the bias term and the URA variance in the existing GEAS error model.

Looking at the results in Table 3, it appears that the iono-free and tropospheric terms have slightly larger contributions towards the overall error than what was modeled previously in simulation. The "Sigma" and "Bias" values in this table represent an average over all measurements in the respective elevation bin (5-15°, 15-25°, 25-35°, 35-45°, 45-55°, 55-65°, 65-75° and 75-90°), while the values on the right represent the modeled error sigmas at the edges of these elevation bins. The standard deviation in the right hand side column corresponds to the sum of the $\sigma_{iono\text{-}free}$ and σ_{tropo} terms. Figure 8 illustrates the same comparison between modeled and observed errors in both receivers onboard the airplane. Possible reasons for the observed differences could be either a peculiarity of this data set, such as higher than expected noise due to the setup and operation of the data collection equipment, or if the theoretical model used was devised based on different assumptions, not applicable to the measurement in this flight inspection test.

The error model assumptions that are most likely to explain the observed discrepancy are the URE mean and variance, which are based on previous measurements at L1, and the multipath model which might prove to be very different in the airborne environment. Significant differences exist between observations of nominal noise levels in the L1 band for carrier-aided code tracking and the actual noise level for the L2 semicodeless acquisition that was employed

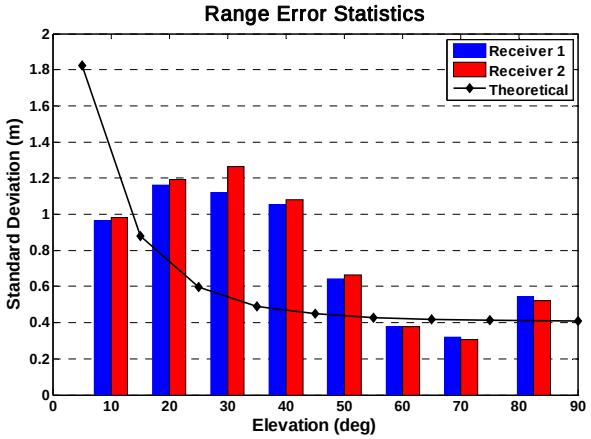

Figure 8. Graphical comparison between the theoretical error model (excluding the URA) and the residual error measured by the two receivers (Ashtech and Novatel).

in the current data set in order to enable dual frequency measurements. It is expected that once modernized GPS signals (i.e. L1C, L2C and L5) are available on all satellites, the expected URE levels will be lower than in L1 today, and thus it is not desirable to devise an overconservative theoretical model based solely on the types of errors observed in L1/L2 positioning in this experiment. Further analysis is warranted in order to determine whether the L2 semicodeless acquisition employed here is the major source of disagreement between the expected and the measured range errors. A careful separation of the errors due to L2 tracking alone needs to be done, after which the validation of the error model will be done based on the error levels at L1 today. This procedure will yield a theoretical model which will be only moderately conservative with respect to future GPS performance, leading in turn to a minimal degradation of performance (i.e. VPL inflation) due to conservatism in modeling errors. Finally, additional investigation in the direction of airborne multipath will be conducted as well before the success of the error model validation will be re-evaluated and a more precise conclusion on the performance of future multi-constellation unaided RAIM will be drawn.

ACKNOWLEDGEMENTS

The first author would like to thank his academic advisor, Prof. David Powell, for meaningful discussions and advice in preparing this work as well as insight on the applicability of current results to aviation approaches. Also to Dr. Juan Blanch for advice during the theoretical development of the RAIM algorithm, and to Dr. Todd Walter for discussions on compatibility of the algorithm results with FAA needs and specifications, and on the significance of current results in the broader context of satellite-based navigation.

Finally, the authors would also like to extend their gratitude to the Federal Aviation Administration for the grant supporting this work and the Stanford University WAAS research efforts. The views expressed in this paper belong to its authors alone and do not necessarily represent the position of any other organization or person.

REFERENCES

ARINC Engineering Services, LLC, *Interface Specification – Navstar GPS Space Segment/ Navigation User Interfaces*, IS-GPS-200D, Navstar GPS Joint Program Office, El Segundo, CA, 7 December 2004.

Blanch, J., Ene, A., Walter, T., and Enge, P., *An Optimized Multiple Hypothesis RAIM Algorithm for Vertical Guidance*, in Proceedings of the ION GNSS 20th International Technical Meeting of the Satellite Division, Fort Worth, TX, 25-28 September 2007.

Ene, A., *Multiple Hypothesis RAIM with Real-Time FDE and Forecasted Availability for Combined Galileo-GPS Vertical Guidance*, in Proceedings of the European Navigation Conference - GNSS/TimeNav, Geneva, Switzerland, 28-31 May 2007.

Ene, A,, Blanch, J., and Powell J.D., *Fault Detection and Elimination for Galileo-GPS Vertical Guidance*, in Proceedings of the Institute of Navigation National Technical Meeting, San Diego, CA, 22-24 January, 2007.

Lee, Y.C., Braff, R., Fernow, J.P., Hashemi, D., McLaughlin, M.P., and O'Laughlin, D., *GPS and Galileo with RAIM or WAAS for Vertically Guided Approaches*, in Proceedings of the ION GNSS 18th International Technical Meeting of the Satellite Division, Long Beach, CA, 13-16 September 2005.

Misra, P., Enge, P., *Global Positioning System: Signals, Measurements, and Performance*, 2nd Edition, Ganga-Jamuna Press, 2005.

Radio Technical Commission for Aeronautics, *Minimum Operational Performance Standards for Global Positioning / Wide Area Augmentation System Airborne Equipment*, RTCA DO-229D, RTCA, Inc., Washington, D.C., 13 December 2006.